The HCO Potential Energy Surface; Probes Using Molecular Scattering and Photodissociation

D. W. Neyer and P. L. Houston

Department of Chemistry
Cornell University
Ithaca, NY 14853-1301

Abstract

The results from three recent types of experiment investigating the interaction potential between a hydrogen atom and a carbon monoxide molecule are summarized and compared to theoretical predictions based on an *ab initio* HCO potential energy surface. In the first experiment, energetic hydrogen atoms generated in the photolysis of H_2S collisionally excite CO molecules to high rotational levels of v = 0, 1, and 2. The product state distributions are compared with the predictions of classical trajectory calculations. In the second experiment, HCO is excited to an upper Renner-Teller component that is degenerate with the ground potential energy surface in the linear configuration. Coupling between the states leads to dissociation, and the CO product distribution is again measured and compared to the predictions of classical trajectory calculations. In the third experiment, HCO is prepared by stimulated emission pumping (SEP) in highly excited vibrational levels above the dissociation limit on the ground state potential energy surface. The SEP linewidths provide information about the rate of dissociation, and a measurement of the CO product distribution provides information about the dynamics. Both experimental observations are compared to results from recent wave packet calculations.

I. Introduction -- The HCO Potential Energy Surface

The formyl radical, HCO, is of importance in combustion,[1,2] atmospheric chemistry,[3] and interstellar space.[4] In addition, because *ab initio* calculations provide accurate energies for a system of such light atoms, HCO has become a prototype system for theoretical studies of radical spectroscopy and unimolecular reactions.

From an experimental point of view, the spectrum of HCO and the interaction between hydrogen atoms and CO have long been of interest. Ramsay first observed and identified the long wavelength HCO absorption spectrum (450-750 nm) in 1953,[5] and subsequent investigations have detailed the nature of this transition from the ground $\tilde{\mathrm{X}}$ ($^2A'$) state to the first excited $\tilde{\mathrm{A}}$ ($^2A''$) state.[6-15] The absorption from the ground $\tilde{\mathrm{X}}$ ($^2A'$) state to the second excited $\tilde{\mathrm{B}}$ ($^2\mathrm{A}'$) state has also recently been characterized.[16-21] The nature of the interaction between H atoms and CO has also been investigated through studies of collisions between these species.[22-25] Such spectroscopic and dynamics experiments provide important insight into the nature of the potential energy surfaces for HCO and the interactions between them.

The earliest *ab initio* potential energy surface (p.e.s.) for the HCO system appears to be that constructed by Bowman, Bittman, and Harding[26] (BBH) based on calculations by Harding[27] and adjusted to agree with experimental data from Murray *et al*.[28] The potential was later fit to a

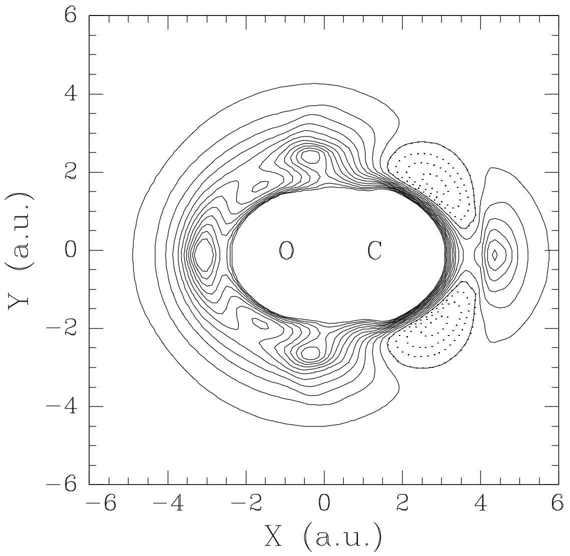

Figure 1 Contour plot of the BBH potential energy surface of HCO for a fixed C-O bond length of 2.25 a.u. The contours are spaced every 0.25 eV with the dashed contours indicating energy below the energy of the H+CO asymptote.

Legendre expansion by Romanowski *et al.*[29] Figure 1 provides a view of this surface for the C-O distance fixed at its equilibrium value. The contours show the energy that a hydrogen atom would experience at various locations relative to the fixed C-O. There are several important features of the potential. First, there is an attractive well (dotted contours) in the two symmetrical bent geometries corresponding to the bound HCO radical. A barrier of about 5500 cm^{-1} leads from either well to free H + CO products. Second, there is a barrier in the linear H-CO configuration between the two symmetric forms of bent HCO. As will be discussed in detail later, at the top of this barrier the ground electronic state shown in the figure becomes degenerate with an excited electronic state (not shown); these two states, the X̃ state and the Ã state, are two components of a Renner-Teller pair. Third, there is a metastable well in the bent CO-H configuration with a geometry approximating that of the methanol framework. A substantial barrier separates this metastable well from the true minimum.

A great deal of theoretical work[26-49] has investigated the properties of the BBH surface[26,29] as well as alternative surfaces.[30,31] Trajectory calculations predicting vibrational and rotational excitation of CO on collision with fast H atoms have been performed to account for experimental observations.[33] The H + CO recombination reaction and its reverse dissociation reaction have been thoroughly investigated, largely because of the importance of this reaction in combustion.[40-44] Perturbations of the B̃ state have been studied.[48] Finally, wavepacket calculations have been performed to model dissociation from both the Ã state and high vibrational levels of the X̃ state,[45-47] and L^2 calculations of resonances on the X̃ surface and of the final rotational distributions following dissociation from these resonances have been also been performed.[49] While it is beyond the scope of this article to review these advances in detail, we note that other chapters in this volume will also cover theoretical approaches to understanding the HCO potential energy surface.[50]

The objective of this paper is to review recent experimental work on the HCO system performed at Cornell and to point to directions for future exploration. The experiments from our laboratory have evolved from state-resolved collisional investigations through studies of the Ã-state photodissociation of HCO to exploration of the dynamics of dissociation from highly excited rovibrational levels of the ground state. All of the studies share a common experimental feature, the sensitive and state-specific detection of CO by vacuum ultraviolet (VUV) laser induced fluorescence (LIF). We begin by describing studies of collisions of H with CO.

II. Scattering Probes of the HCO Potential

The scattering dynamics of the H+CO system have been the subject of several experimental[23-25] and theoretical investigations.[27-39] As mentioned above, the great interest in this particular system has been sparked by the availability of good *ab initio* calculations.[26,27,30] Trajectory calculations performed on the BBH surface have been used to describe high-energy scattering,[33] and several quantal studies have examined collisions at energies corresponding to metastable resonances.[34-38] A time-correlation function approach was applied by Micha *et al.* to H+CO scattering at 1.6 eV.[39]

From the experimental point of view, there has been substantial interest in collisions of fast hydrogen atoms with small molecules.[51] The experimental attraction is that the H atoms can be generated conveniently by photolysis of hydrides such as HBr, HI, and H_2S. The technique has the advantages that the H atoms are nearly monoenergetic and that the collisions occur at energies high enough to probe chemically interesting regions of the potential surface. Both inelastic and reactive scattering processes have been studied. Most scattering experiments have determined integral cross sections with various levels of state resolution, but some recent experiments have begun to explore differential cross sections as well.[52-55] Work in this field prior to 1987 was reviewed by Flynn and Weston.[51] In the case of H+CO, the vibrational populations of CO after collision with 2.3 eV H atoms were previously measured by Flynn *et al.* and by Leone *et al.* using infrared fluorescence.[23-25] Our own group has obtained rotationally state-resolved populations at 1.6 eV and 2.3 eV for the *v*=0, 1, and 2 levels and has interpreted the results both through surprisal analysis and by comparison with trajectory calculations on the BBH surface.[56,57]

Figure 2 shows a region of the laser-induced spectrum of CO following collisions with 2.3 eV hydrogen atoms. It is clear from the spectrum that the collision produces very high rotational levels of *v*=0 as well as substantial population in low rotational levels of *v*=1. The experiment was performed by expanding a mixture of CO and H_2S in a supersonic free jet, so that the initial CO was primarily in *v*=0 and very low *J*. Hydrogen atoms produced by the dissociation of H_2S with an ultraviolet laser pulse collided with the CO, which was detected 75 ns later using laser induced fluorescence on the A←X transition. The vacuum ultraviolet light needed to excite this transition was generated by four wave mixing in magnesium vapor, where one laser at 430.8 nm excited a two photon resonance and a third photon at the wavelength indicated on the upper axis of Figure 2 was

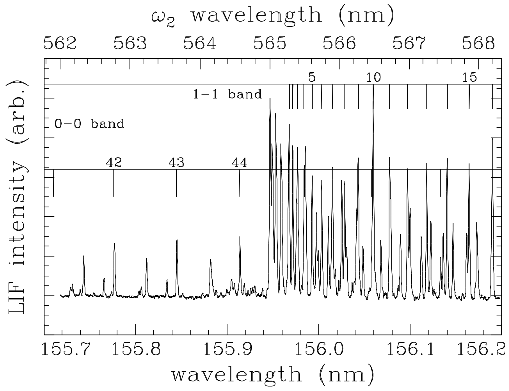

Figure 2 Region of the experimental spectrum showing high-J lines of the (0,0) band and the (1,1) bandhead. Q-branch transitions are identified in the figure. The (4,3) bandhead is also just observable near the Q(44) line of the (0,0) band.

used to generate the wavelength indicated on the lower axis. Further experimental details are provided in ref. 57.

The experimental results for CO produced in vibrational states *v″*=0, 1, and 2 are shown in Figure 3, which also displays the results of trajectory calculations performed on the BBH potential energy surface. The average of all measurements for each level is plotted with error bars representing 80% confidence limits. The spectra which determine populations for *J*≤17 of the ground vibrational state were taken with samples of CO and H_2S seeded in argon. The results of the seeded and unseeded experiments were identical in the region of overlap between *J*=10 and *J*=20.

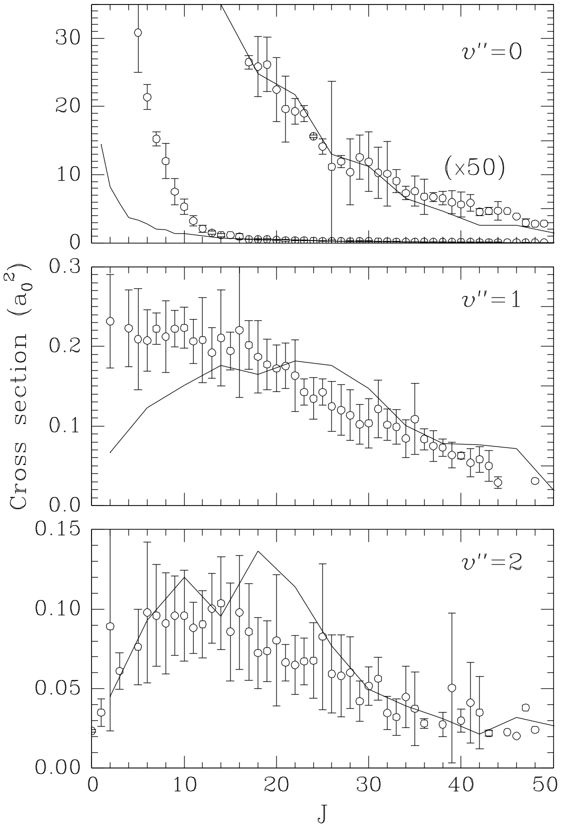

Figure 3 Relative populations for *v*=0, 1, and 2 scattered CO. Error bars give 80% confidence limits calculated from multiple measurements; points without bars were measured only once. The circles give the experimental measurements, while the solid line gives the result predicted by the classical trajectory calculations. The experiments were scaled to the theoretical cross sections over the range *v*=0, J≥16, as shown in the expansion. The experimental results for *v*=1 and 2 were scaled using the same factor as for *v*=0.

The solid lines give results of classical trajectory calculations performed on the BBH potential energy surface. Since the experiments determined only relative cross sections, it was necessary to scale the results for comparison with the trajectory calculations. The scale factor was chosen to provide good agreement in the $18 \leq J \leq 50$ region in *v*=0. In general, the calculated rotational distributions and the data agree quite well with two notable exceptions. First, there is a very sharp increase in cross section in the experimental results not matched by the calculations for *J*<15 in *v*=0.

At J=5, for example, the experimental cross section is roughly four times the calculated one. Second, for v=1 the cross section variation as a function of J is roughly flat from J=0 to 12 in the experimental results, while it drops off below J=15 in the calculations. We discuss these two observations next.

The low-J cross sections are the most serious source of disagreement between theory and experiment. Collisions responsible for these small ΔJ transitions are most likely grazing collisions having large impact parameters. However, it is not the case that these collisions have their turning points, or distances of closest approach, in regions not treated accurately by the BBH potential. We have examined carefully the distribution of turning points in our trajectory calculations. Collisions which produce $J\leq 20$ have inner turning points outside the HCO and COH well regions, but not so far out as the van der Waals well region. We find that the distance between the H and the center of mass of the CO at the inner turning point of each trajectory which leads to $3\leq\Delta J\leq 10$ is always less than 5.0 a_0 and usually closer to 4 a_0. Such collisions sample interaction potentials that are always above 0.2 eV. We conclude that the BBH surface could be the origin of the discrepancy between theory and experiment only if the surface is defective in the 4-5 a_0 region, where trajectories producing $3\leq\Delta J\leq 10$ have inner turning points.

A number of experimental sources for the discrepancy between theory and experiment are possible, including multiple collisions of the CO molecules with other species and multiple collisions of the H atoms with different CO molecules. However, careful examination of these possible problems[57] leads to the conclusion that neither is likely and that, even if present, neither would be likely to lead to the observed discrepancy. A remaining possibility that collisions of H atoms with Ar-CO clusters might cause an increase in production the low-J CO products has not definitively been ruled out.

The smaller discrepancy between the experimental and calculated rotational distributions for v=1 has been ascribed to an inaccurate description of the HOC saddle point region on the BBH surface. When the surface was generated, spectroscopic data on HCO were used to adjust the surface in the HCO well region. No data were available on HOC, so the surface in that region was fit to the unadjusted *ab initio* energies. Those energies are probably a little (~0.2 eV) too high, so in the trajectory calculations it is a little too hard for trajectories to sample the HOC well region. Trajectories reaching this region have a high probability of producing CO in v=1 because there is strong coupling between C-H and C-O motions in this region of the potential. They also produce low rotational levels because the hydrogen atom strikes the CO near its center of mass. In preliminary calculations, lowering the barrier to the COH well by 0.2-0.4 eV resulted in enhanced cross sections for low J (J<5) of CO(v=1) without changing the cross sections for larger J.

In conclusion, several detailed observations about the dynamics of H+CO scattering were made in this collisional study. T→V transfer between H and CO at 2.3 eV is dominated by dynamics occurring in the two wells on the HCO surface. The HCO well, which corresponds to a bound HCO molecule, is more important since the great majority of vibrationally inelastic trajectories pass through this well. The HCO well provides the easiest approach for an H atom to the regions of the surface where it can impart a significant impulsive force on the CO oscillator, but the basic character of the CO triple bond remains essentially unchanged during the collision.

The COH well, on the other hand, can be reached only by crossing a high barrier. The potential is not as steep on the inner wall of the COH well as it is in the HCO well, but the COH radical has a much longer CO bond at its minimum-energy configuration. The change in equilibrium bond length as the H atom moves from the COH saddle point to the COH well provides strong coupling to higher vibrational states, without a strong tendency to excite high rotational levels.

The BBH surface describes H+CO scattering in the region of the HCO well very accurately. This accuracy is reflected in the good agreement between calculated and observed relative vibrational cross sections for $v \geq 1$, for the rotational distribution in v=2, and for the high-J rotational distribution in v=1. However, the contribution from collisions reaching the COH well at 2.3 eV is underestimated in trajectories on the BBH surface. The COH saddle point is probably a little too high on this surface, so that fewer trajectories access the region between the saddle point and the metastable well where vibrational excitation is induced.

There is also a discrepancy between theory and experiment with regard to the cross sections for low J states in vibrationally elastic scattering. This difference could be due to an error in the BBH surface, but if it is, it would have to be associated with geometries where the *ab initio* calculations should have been accurate. As we will see later, there are some indications that the barrier to H + CO recombination is not high enough on the BBH surface, and this change may influence the low J results. Experimental sources for the discrepancy also need further investigation.

III. Probes Using Photodissociation through the *Ã*-state

Another method for probing the HCO p.e.s. is to examine its photodissociation. The lowest electronic transition of the formyl (HCO) radical, between the $\tilde{X}\ ^2A'$ and the $\tilde{A}\ ^2A''$ states, has been the focus of many spectroscopic investigations. The "first definite spectroscopic evidence for the existence of the HCO radical"[6] has been attributed to the $\tilde{A}\leftarrow\tilde{X}$ absorption experiments of Ramsay[5] in 1953. From the results of Ramsay's absorption experiments[6-8], as well as from other studies of the $\tilde{A}\leftarrow\tilde{X}$ transition,[10-15] many of the geometric and spectroscopic parameters of these two states have been determined. For example, it was determined that the ground electronic state of HCO has a bent equilibrium geometry (HCO angle of ~120°), while the Ã state is linear. It was also observed that excitation levels in the Ã state led to predissociation. It is this photodissociation process that has been the main interest of our continued studies of the Ã state of HCO to be described below.

The first evidence of predissociation was the observation of a series of absorption bands that alternated between having diffuse and structured spectra depending on the number of bending quanta excited in the Ã state. States with an even number of bending quanta (v_2) were diffuse, while those with odd values of v_2 had structured bands that could be rotationally assigned to quantum numbers denoted by N.[6] Closer examination of the vibrational bands[7] showed that odd-numbered bending states have diffuse bands as well as structured ones depending on the quantum number K', which describes the projection of the total angular momentum onto the a inertial axis. In HCO, the a axis is nearly parallel to the CO bond, and for the Ã state the K' quantum number is equal to $|\Lambda + l|$, where $\Lambda=\pm1$ is the projection of the electronic angular momentum on the a axis, and l is the vibrational angular momentum of the degenerate bend. Rotational structure was observed only in bands with $K'=0$, and these are present only in levels with an odd number of bending quanta.

The predissociation of the Ã state was attributed to a Renner-Teller interaction with the X̃ state of HCO.[7] A Renner-Teller pair is formed when two electronic states that are degenerate in the linear configuration split in energy as the molecule bends.[58-60] In the case of HCO, the X̃ state decreases in energy while the linear Ã state increases in energy as the molecule bends from a degenerate $^2\Pi$ state. Because the ground state of HCO has only a weak H--CO bond, all Born-Oppenheimer levels of the Ã state are above the dissociation energy, and coupling between these levels and those of the X̃ state results in dissociation.

Renner-Teller coupling depends strongly on the K' quantum number, and only states with K'=0 should be free of predissociation effects. However, careful study of the N-dependent linewidths[8,13,14] of the K'=0 bands revealed predissociation within these bands as well. Some of the line broadening has been attributed to Coriolis effects, while some is attributed to K-type resonances. In addition, a constant homogeneous broadening has been found for all values of N', but the origin of this broadening is unknown.

A theoretical picture for the dynamics of this Renner-Teller interaction has been provided by Dixon.[61] By conducting time-dependent calculations on a pair of simplified one-dimensional bending potentials for the two Renner-Teller states, Dixon found that a wave packet initially confined to the upper electronic state splits between the two surfaces when it reaches the degenerate linear configuration. Assuming the lower state was promptly dissociative, he was able to produce an empirical formula which predicted the lifetimes (and therefore linewidths) of the levels of the Ã state as a function of v_2' and K'. At the time, the prediction was supported by a limited set of linewidths for different v_2' states from absorption experiments. Recent measurements for a larger number of v_2', K' states (described below) are also in good agreement with the predictions of Dixon's treatment.

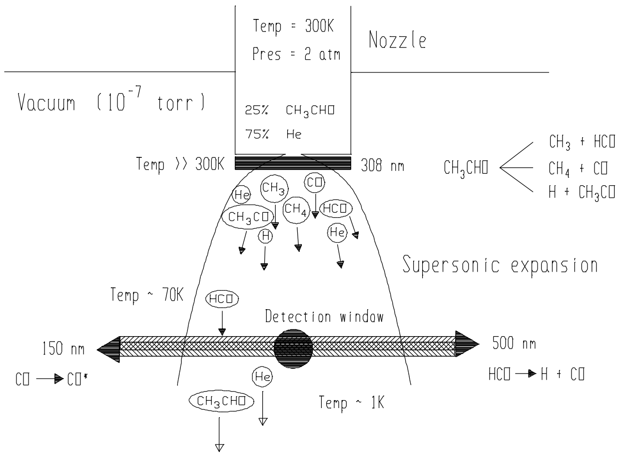

Figure 4 Side view of the nozzle showing the spatial overlap of the three laser beams. Some conditions relevant to the supersonic expansion are also indicated.

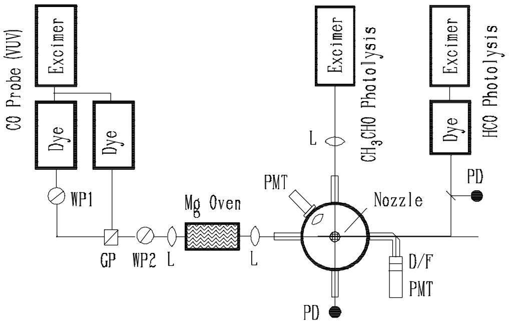

Figure 5 Physical layout of the experimental apparatus (top view). The nozzle is directed into the plane of the figure. BS=beam splitter; D=diffuser; F=visible filter; GP=Glan-Taylor prism; L=lens; PD=photodiode; PMT=solar blind photomultiplier; WP1=half-wave plate; WP2=quarter-wave plate.

In order to confirm the dissociative nature of these Ã state transitions and to understand the dynamics of the dissociation process, we conducted a series of experiments[62-65] in which the CO products were detected by laser-induced fluorescence. The experiments have been described in detail previously.[63] Briefly, as shown in Figure 4, a free jet expansion of acetaldehyde is photolyzed at the nozzle orifice with an ultraviolet laser to create HCO radicals. The radicals are cooled in the subsequent expansion, and, downstream, a visible laser (450-750 nm) excites the HCO to the dissociative Ã state. The CO photofragments are probed approximately 50 ns later with a VUV laser produced by four-wave mixing in Mg vapor. A schematic of the experimental setup is shown in Figure 5.

The detection of CO fragments from the excitation of HCO has confirmed that the Ã state is predissociative. In general, the CO products which come from these predominately bending levels of the Ã state are rotationally excited with rotational distributions peaked around J=30. To understand the detailed product state distributions measured in these experiments, one can picture the dynamics in terms of a time-dependent three-step process: (1) excitation of specific levels of the Ã state, (2) crossing from the Ã state to the X̃ state, and (3) dissociation on the X̃ state potential energy surface.

As discussed above, excitation of levels in the Ã electronic state can be accomplished with vibrational resolution and with selection of specific K states. The excited levels are described by the notation, (v_1,v_2^K,v_3), where v_1, v_2, and v_3 describe the number of quanta in the H-CO stretch, the HCO bend, and the HC-O stretch, respectively, and K has been defined previously. Detection of the CO dissociation product allows one to perform spectroscopic measurements of the Ã←X̃ transition which are not possible in more conventional spectroscopic methods. The technique we have used is known as photofragment excitation (PHOFEX) spectroscopy and involves monitoring a specific product state [in this case CO(v,J)] as a function of the wavelength of the laser exciting the HCO. The spectra record the excited state of the parent molecule (similar to absorption or LIF), but the intensity of individual transitions is determined by a combination of the absorption strength and the yield of fragments in the specific state being monitored. The PHOFEX technique allows one to bias the detection to reveal transitions that are hidden in other measurements. In the case of HCO, this technique is particularly advantageous since diffuse, dissociative transitions are inherently weak in LIF measurements but can be enhanced in PHOFEX spectra. In addition, transitions which have weak oscillator strengths, but which produce distinct product states, can be observed with PHOFEX techniques even though they are often lost in the baseline or congestion of absorption spectra.

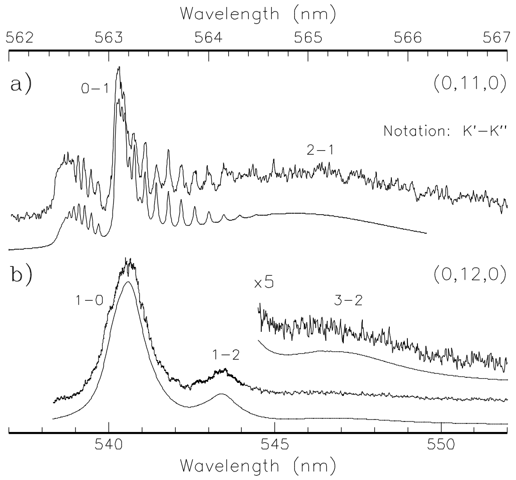

Figure 6 Detailed HCO PHOFEX spectra showing representative sharp and diffuse rovibronic bands. K-subbands are labeled as K′-K″; Simulated spectra used to infer homogeneous linewidths are shown beneath the experimental spectra.

PHOFEX spectra for the (0,11,0) and (0,12,0) bands with the assigned *K* subbands are shown in Figure 6. The dominant peaks in a spectrum obtained by monitoring the CO(v=0, J=30) product are those corresponding to $\tilde{A}(0,v_2,0)\leftarrow\tilde{X}(0,0,0)$ transitions which have the largest oscillator strengths. The positions of these peaks have been compared to the absorption measurements of Brown and Ramsay.[8] The bandhead positions of the sharp (K'=0) bands match quite well, while the positions of the diffuse bands are consistently shifted from the absorption measurements. This is probably due to a difference in rotational temperature of the HCO sample. The Brown and Ramsay experiments were performed in a room temperature bulb while the measurements of Loison *et al.*[63] employed a free jet expansion.

When different product states of CO are monitored, PHOFEX spectra can reveal new transitions. For example, if CO(v=0, J=50) is monitored, a series of combination bands is observed due to excitation of $(1,v_2,0)$ levels observed only weakly in absorption. As will be discussed below, dissociation from these C-H stretching bands produces more rotational excitation in the product CO than does dissociation from purely bending states. Similarly, previously hidden combination bands from excitation of $(0,v_2,1)$ states are revealed when CO(v=1, J=30) is monitored. In addition, the PHOFEX technique has allowed transitions to states with higher values of K′ to be observed.

Although absorption measurements have revealed the energetic positions of many of the transitions described, accurate linewidth measurements of these states had not been obtained. Laser induced fluorescence has been able to measure the linewidths of the K=0 states, but is ineffective for the strongly predissociative levels with $K'>0$. One of the main accomplishments in applying PHOFEX spectroscopy (which is biased in favor of dissociative states) to the HCO(Ã←X̃) transition has been the measurement of linewidths for a large collection of (v_1,v_2^K,v_3) levels.[63] Experimentally, the linewidths within a given vibrational state increase as K' increases. For a given value of K', the linewidths decrease as the number of bending quanta excited, v_2, increases. There is essentially no change in linewidth when one quantum of C-O stretch is added to the excitation of a pure bending state, and only a small effect when one quantum of C-H stretch is excited (the linewidths become 10-20% broader). Measurement of the linewidths of DCO show them to be narrower than those of HCO when the comparison is made with the same values of v_2 or with comparable amounts of energy in the bend.

An explanation of the trends in these linewidth measurements involves the second step in the dissociation process -- the crossing from the Ã state to the X̃ state. To understand this step, we look more closely at the Renner-Teller based model developed by Dixon using wave packet calculations.[61] In his treatment, Dixon used very simple one-dimensional harmonic oscillator functions to describe the bending potential for each of the two electronic states. The higher energy surface was a bound harmonic oscillator, while the lower potential was modeled with an inverted parabola. The two potentials were degenerate in the linear configuration (the minimum of the upper surface). A wave packet initially describing an excited bending level on the upper state was propagated in time using a Hamiltonian with a K-dependent Renner-Teller coupling between the two surfaces. Dixon found that the wave packet remained primarily on the upper state until it approached the linear configuration where the Renner-Teller coupling is strongest. The wave packet then split, and a portion of it continued on the lower state. Since the lower potential was an inverted parabola, the part of the wave packet propagating on this surface continued directly away from the linear configuration toward "dissociation." Since the dissociation step in this model is direct and fast, the rate-limiting step is the crossing from the upper to the lower potential, and this crossing rate determines the linewidths of the transitions.

Dixon's model predicts that population on the lower potential energy surface is produced in the region near the linear configuration. The calculations also allowed Dixon to formulate an empirical rule for the linewidths of the $\tilde{A} \leftarrow \tilde{X}$ transitions of HCO. The linewidths depend on the values of v_2' and K' excited in the transition, as well as the force constants of the upper and lower harmonics oscillators, described by the parameters f′ and f″, respectively.

The linewidths of the HCO($\tilde{A} \leftarrow \tilde{X}$) transitions measured using the PHOFEX technique are shown in Figure 7 for several values of v_2' and K', along with those measured for DCO. The solid lines in the figure represent the results from Dixon's model with just one adjustable parameter, f″. The value of f′ was calculated from the nearly harmonic bending frequency determined spectroscopi-

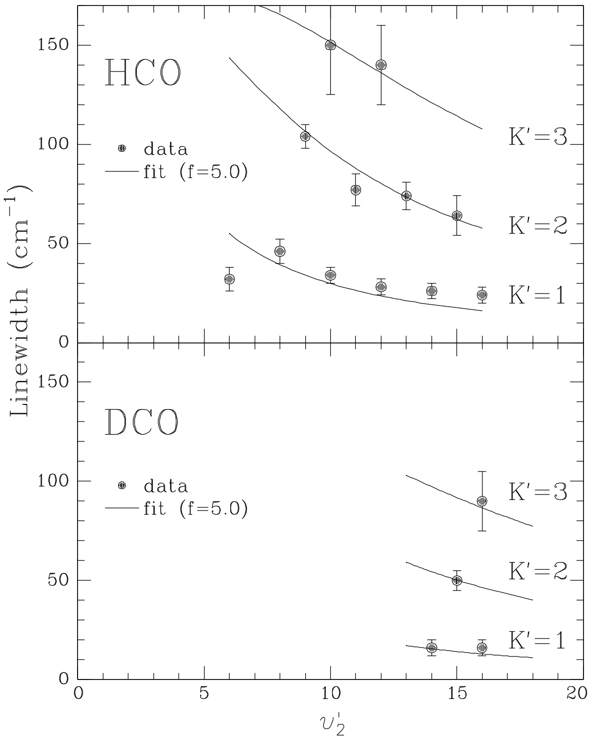

Figure 7 The linewidth plotted against υ_2' for each value of K′ for HCO and DCO. The solid lines are calculated using Dixon's model.

cally for the Ã state. The best-fit value of f″=5.0 provides very good agreement with almost all of the experimental data, including the DCO data in which the only parameter change is the different reduced mass. The main discrepancy occurs in the linewidth of the HCO v_2'=6, *K*′=1 state and has not been explained.

In addition to the excellent agreement with experimental linewidths, Dixon's model is further supported by the data of Figure 8, which shows the CO rotational distributions for similar bending states with different values of *K*′. Even though these states have very different lifetimes, their product state distributions are nearly identical. These results support the idea that the crossing takes place in a very localized region of the potential (near the linear configuration), and that although the rate of crossing can be quite different, the region of crossing is the same. The product state distributions are determined by the vibrational partitioning of energy at the linear crossing region and by the energy redistribution caused by the ground state potential energy surface.

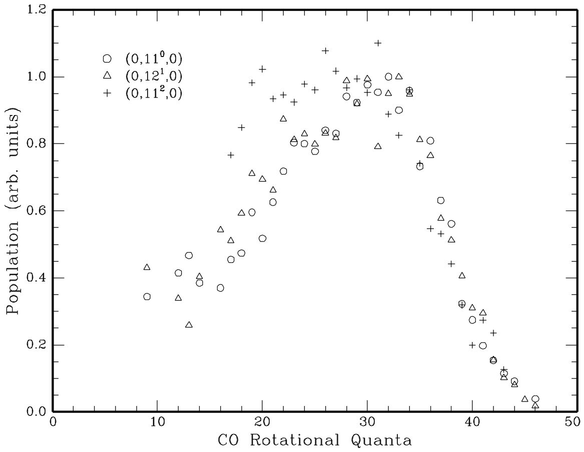

Figure 8 Rotational distribution of CO(v=0) produced from the Ã-state dissociation of HCO with differing initial values of *K*′.

A classical picture is helpful to understand this final step of the dissociation process -- energy redistribution on the X̃-state p.e.s. Indeed, classical trajectory calculations,[65] as well as more recent wave packet calculations,[47] have simulated the dissociation and produce fairly consistent results. In the classical model,[65] it was assumed that the C-H and C-O stretching motions initially excited in the Ã state are preserved when the HCO reaches the linear crossing point, and that since these stretching modes have at most one quantum of excitation, they are adequately described as harmonic oscillators. Because all of the accessible Ã state levels have significant amounts of bending energy and the crossing takes place in the linear minimum of the upper surface, the system has a considerable amount of bending angular momentum as it starts its trajectory on the ground state surface. Closer examination of three regions of the BBH potential energy surface (Figure 9) will help illustrate what happens to this initial energy as the HCO molecules dissociate.

The first region of the p.e.s. that significantly affects the dissociation dynamics is the narrow channel leading away from the linear region of the surface. This channel allows the original bending motion to become angular momentum of the H around the CO while maintaining a bound C-H stretching motion. The calculations are sensitive to the height of the linear isomerization barrier with respect to the separated H and CO fragments since it determines the overall energetics of the trajectory. In addition, the initial steepness of descent and narrowness of the channel will determine how much of the energy will be divided between bending motion and C-H stretching.

The second important region of the p.e.s. is near the HCO well. On the BBH potential, the bending channel leads directly into this overall minimum of the surface, corresponding to the bent geometry of ground-state HCO. As the H atom enters this region it continues to gain angular momentum, but once it crosses the bottom of the well the momentum decreases as the H atom ascends the other side. Another important aspect of the well region is that the C-H stretching potential has become much wider than it was in the original bending channel. The very anharmonic C-H stretching mode is essentially the dissociation coordinate, and coupling of the bending motion into this coordinate is quite important in determining the dynamics.

The third important region of the p.e.s., the exit channel, is the section of the potential surface over which the trajectory must pass to break the chemical bond. In the case of HCO, we see that there is a narrow angular range (~100° < ∠HCO < ~150°) of the ground state well in which dissociation can take place over a rather low and isotropic barrier. Outside this range of angles, the barrier rises sharply to form on one side a "knob" in the potential (at a bending angle of about 90 degrees) and on the other side the narrow bending channel described above. The knob is actually the isomerization barrier between HCO and COH, and the position and steepness of the barrier appears to have a substantial effect on the final states produced in the CO fragment.

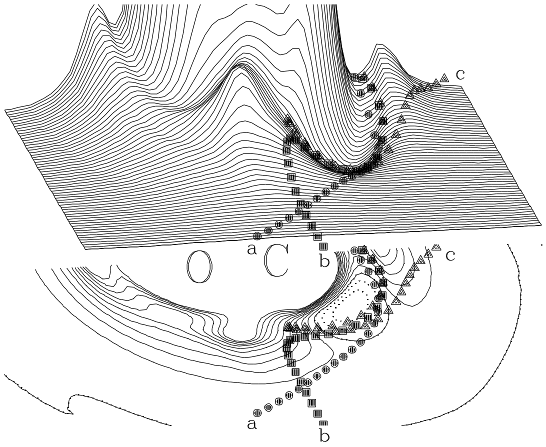

Figure 9 Three-dimensional surface plot and contour map of the BBH ground state potential energy surface of HCO. The plots are for a fixed C-O bond length of 1.19 Å (2.25 a_0) and show the potential felt by the H atom in the cartesian space around the C-O. The surface is axially symmetric about the linear HCO axis (the back edge of the plots). The contour lines are spaced by 0.25 eV, with the dotted lines indicating energies below the asymptotic zero of energy corresponding to a separated H atom and CO molecule. Overlayed on each plot are three calculated trajectories originating along the linear axis of the HCO and leading to dissociation. The final rotational state of the CO for each of the trajectories is: (a) J=31, (b) J=0, and (c) J=23.

When an ensemble of classical trajectories is run starting in the linear configuration, a variety of paths to dissociation is found. Three of these paths are shown in Figure 9. Path **a**, which goes through the bent well of the potential and over a low dissociation barrier (missing the knob), is typical of most of the trajectories calculated. This path produces a CO fragment with a significant amount of rotational energy (J=30). Some of the trajectories go through the well, but then hit the knob, as shown in paths **b** and **c**. For the trajectories similar to **b**, the knob decreases the angular momentum of the H atom around the CO and channels that energy into translation leaving the CO in a low rotational state (J=0).

Trajectories similar to path **c**, however, roll back down through the well and regain angular momentum (now with opposite sign) before dissociating. This third type of trajectory also produces rotationally excited CO (*J*=23), but rotating in the opposite direction of the CO produced in path **a**. One can see that the size and position of this HOC isomerization barrier determine the number of trajectories that escape from the well unhindered and the number that hit the knob and change path dramatically. In addition, the slope and shape of the barrier determine whether the trajectories follow paths similar to **b** or **c**.

Measurement of the final CO product state distributions for the dissociation from a variety of Ã state vibrational levels allows us to learn about the energy redistribution processes in the HCO dissociation. Comparison of these results with trajectory calculations using the BBH potential provides a detailed test of those parts of the surface described above. In general, the CO product distributions measured in experiments are rotationally excited (with peaks near *J*=30) and vibrationally unexcited (predominately in *v*=0). Since the excited parent levels are all created with significant bending motion, it appears that the rotational excitation of the products is caused by transformation of bending into rotation, but the knob on the surface limits how much angular momentum can be gained. Because the final rotation is limited, much of the available energy appears in translation of the fragments.

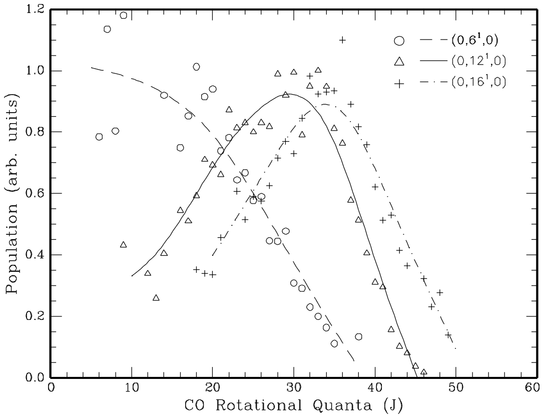

Figure 10 Rotational populations of CO(v=0) from the dissociation of HCO in the Ã(0,n,0), n=6,12, and 16 levels. The overlayed lines are smoothed fits to the data.

Figure 10 shows that excitation of Ã states with an increasing number of bending quanta produce CO fragments with increasing rotational excitation. This observation is consistent with the rather intuitive picture described above. Somewhat surprisingly, excitation of C-H stretching motion in the parent also produces a substantial increase in CO rotational motion. Figure 11a shows the experimental CO(v=0) rotational distributions for the dissociation of the (0,9,0) and (1,9,0) states of HCO. On average, about 60% of the energy originally deposited in the C-H stretch is transformed to rotational energy in the CO fragments. Finally, the C-O stretch in the parent HCO appears to be a spectator to the dissociation process. Comparison between dissociation from the $(0,12^1,0)$ and $(0,12^1,1)$ levels of HCO reveals that the dominant product for the purely bending level is CO(v=0), while the combination band produces predominately CO(v=1). The rotational distributions for these

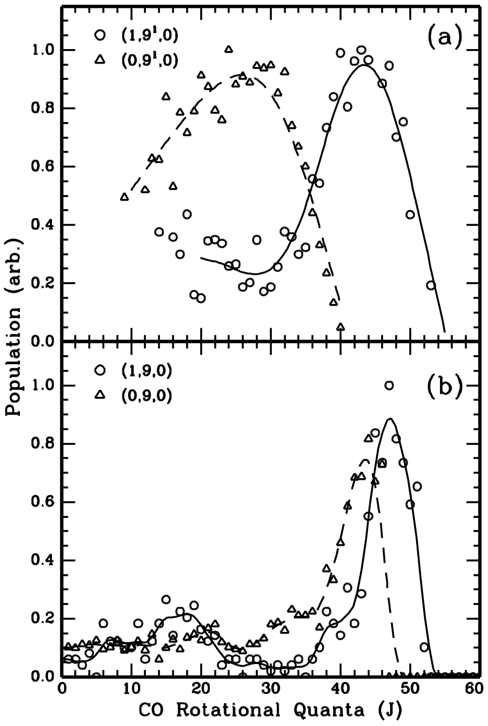

Figure 11 Rotational populations of CO(υ=0) from the dissociation of HCO in the $\tilde{A}(0,9^0,0)$ and $\tilde{A}(1,9^0,0)$ states. The experimental measurements are shown in (a) and the results of classical trajectory calculations are presented in (b). There is no analogue to the K quantum number in the planar calculations. The overlayed lines are smooth fits to the data.

products are shown in Figure 12 and are essentially identical. It appears that the energy originally deposited in the HC-O stretch remains in the C-O stretch during the dissociation, producing vibrationally excited CO without affecting the other dynamics.

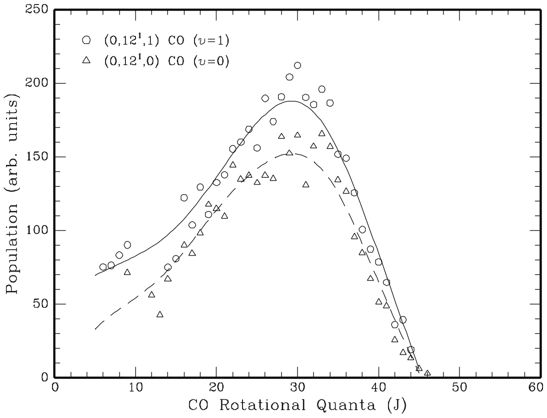

Figure 12 Rotational populations of the dominant vibrational level of CO from the dissociation of HCO in the $(0,12^1,0)$ and $(0,12^1,1)$ vibrational levels of the Ã electronic state. The overlayed lines are smooth fits to the data.

Both classical trajectory calculations and wave packet calculations have been completed in an attempt to model the HCO system. The classical trajectories (described above and in reference 65) were calculated on the BBH ground state potential energy surface starting at the linear crossing region. The time-dependent quantum mechanical methods of Goldfield, Gray, and Harding[47,50] treated the entire Renner-Teller process using the BBH ground state p.e.s. along with a detailed Ã state surface. The wave packet calculations did not, however, treat the C-O stretching degree of freedom. In general, both sets of calculations predict more rotational excitation in the CO products than is observed experimentally. The trend of increased CO rotational excitation with H-CO bending motion is modeled reasonably well. Calculations for the dissociation from C-H stretching combination bands in both treatments agree qualitatively but differ quantitatively with the trends measured in experiment. The results of the classical trajectory calculations for such levels are shown in Figure 11b. While adding C-H stretch to a bending mode does increase the final CO rotational state distribution, the increase is smaller than that observed in the laboratory, implying that the surface does not couple these motions with enough efficiency. Classical trajectory calculations also indicate that the C-O stretch of the BBH surface is more strongly coupled to the other degrees of freedom than is consistent with experiment. Finally, trajectory calculations for dissociation from purely bending states of HCO predict more vibrational excitation in the CO products than is measured experimentally, and calculations for dissociations from combination bands such as (0,12,1), while showing increased vibrational excitation in the products, indicate CO(v=0) is still the dominant product. As mentioned previously, experiments show that CO(v=1) is the strongest channel. The consistency of results from the two sets of dynamical calculations employing different models and methods indicates that, while many of the qualitative trends in the dynamics are correctly predicted, there are some inaccuracies in the BBH potential surface.

Additional information about the HCO photodissociation comes from measurement of Doppler profiles for the photofragments.[64] The measured anisotropy parameter, β, indicates a recoil distribution of fragments which is nearly parallel to the excitation laser polarization. This is somewhat surprising since the transition is known to be perpendicular to the plane of the triatomic and therefore perpendicular to the breaking bond. It was also found that the magnitude of β depends not only on the value of K', but also on the value of K'' (the angular momentum projection in the initial HCO ground state). A treatment based on the Renner-Teller mechanism has been used to explain these results and is discussed in detail elsewhere.[64] Briefly, the observation of a parallel transition results from the facts 1) that the HCO molecule rotates about its *a* axis rapidly compared to dissociation and 2) that the final H atom trajectory is nearly perpendicular to the CO axis. Thus, while the laser initially excites a perpendicular transition, the H atom recoils with a substantial velocity component parallel to the laser polarization.

The width of the CO(v,J) Doppler profiles has also been used to measure the translational energy of the fragment and to calculate the bond energy of ground state HCO.

The value of 5300±200 cm^{-1} obtained is consistent with the more accurate value of 5492±67 cm^{-1} determined by Chuang, Foltz, and Moore.[66]

In summary, the measurement of photofragment product state distributions following the excitation of HCO $\tilde{A}(v_1,v_2^K,v_3)$ levels has provided considerable insight into the dynamics of this system. PHOFEX spectroscopy has confirmed that the broadening of the Ã-state levels is due to predissociation and has allowed accurate linewidth measurements to be made for these diffuse bands. The excellent agreement of these linewidth measurements with the predictions of Dixon supports his model of such Renner-Teller systems. From this model one concludes that the rate-limiting step in the HCO dissociation is the crossing to the $\tilde{X}$ state, and that the product states are mainly influenced by the energy redistribution on the ground state potential energy surface. The experiments sensitively probe the section of the $\tilde{X}$ state surface from the linear geometry out through a bent dissociation channel. Dynamical calculations on the *ab initio* ground state surface of Bowman, Bittman, and Harding result in product state distributions which are qualitatively in agreement with experiment and which reproduce many of the trends measured for dissociation from different initial states of the parent HCO. There are, however, quantitative disagreements between the experiments and calculations. The calculated CO distributions are consistently too rotationally excited, and there appears to be insufficient coupling of the H-CO stretch into product CO rotational excitation. Conversely, experiments indicate that the C-O stretch is a spectator to the dissociation, while calculations with the BBH surface allow much more transfer of this energy into other degrees of freedom.

Some sections of the BBH potential have been identified on which slight modifications may have a significant influence on the dynamics. More recent spectroscopic studies of the ground state surface have also found discrepancies with the BBH surface and have led to refinements.[18,19] Further dynamical probes are also underway in which the X̃ state is accessed directly by stimulated emission pumping. These experiments are discussed in the next section.

IV. Probes using Photodissociation on the X̃-State

As we have just examined, the ground state potential energy surface for HCO has been studied using the dynamical probes of H+CO collisions and Ã-state photodissociation. The collision experiments sample all geometries of the potential energy surface with a variety of center of mass energies and total angular momenta. The Ã-state photodissociation experiments allow the probing of a very specific region of the p.e.s. (starting in the linear geometry) at a fixed total energy and low total angular momenta, but they include the complication of the Renner-Teller crossing of electronic surfaces. One would like to use dynamics to probe selected regions of the potential energy surface with well-defined energy and angular momentum, but without the effects of a second electronic state. The recent discovery of laser-induced fluorescence from the B̃ state[18] and the applicability of stimulated emission pumping (SEP) to the HCO system[19] have allowed such experiments to be undertaken.

Fluorescence from the B̃ state of HCO was actually the first spectroscopic measurement made on the system. Vaidya[16] detected the fluorescence in the flames of ethylene in 1934, but did not assign the bands to HCO until later.[17] Surprisingly, it was not until 1991 that Sappey and Crosley[18] published the first study of laser-induced fluorescence from the B̃ state. Continued spectroscopic investigations[19-21] have provided a more detailed understanding of this excited electronic state. Sappey and Crosley also examined the dispersed fluorescence to the ground electronic state and found a series of metastable resonances reaching more than 10,000 cm^{-1} above the dissociation limit of HCO. Adamson *et al.*,[19] were able to use stimulated emission pumping to identify further some of these dissociative states, measuring their linewidths and spectroscopic constants. The existence of such resonances was also predicted by the groups of Bowman and Wagner based on quantum mechanical H+CO scattering calculations on the BBH potential energy surface.[43,44]

In an effort to understand the HCO system more completely, a series of dynamics experiments has been conducted to measure the product state distributions arising from the decay of these metastable resonances.[67] As in the Ã-state experiments previously described, a molecular beam of rotationally cooled HCO was formed by photolysis of acetaldehyde. Instead of exciting HCO to the Ã state, two lasers were used to perform stimulated emission pumping through the B̃ state so as to prepare the metastable levels on the ground p.e.s. The decay of these states leads to the production of CO which can again be probed state-specifically using VUV LIF. Due to the Franck-Condon factors controlling the B̃→X̃ transition, the metastable levels prepared have predominately C-O stretching character. Some combination bands involving bending levels can also be prepared. Figure 13[68] shows an LIF spectrum of HCO and a fluorescence depletion SEP spectrum measured while exciting one rotational transition in the pump.[69]

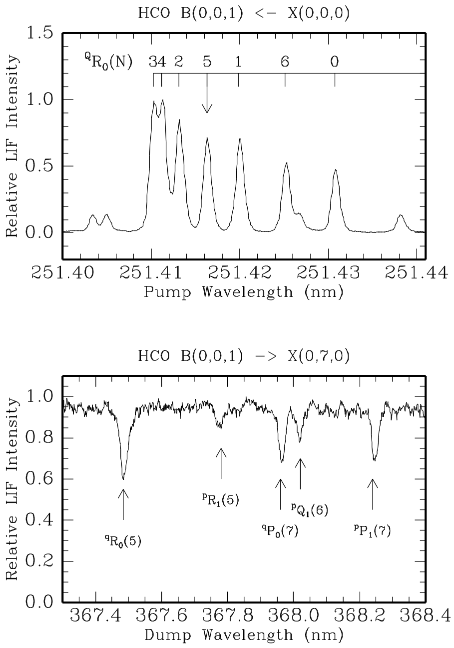

Figure 13 **(a)** $\tilde{B}^2A'\leftarrow\tilde{X}^2A'$ laser-induced fluorescence spectrum of HCO produced by dissociation of acetaldehyde and cooled in an expansion with helium. The $^{Q}R_0(N)$ branch of the transition from the vibrational ground state to the first excited HC-O stretching vibration is identified. The $^{Q}R_0(5)$ pump transition was used for the SEP spectrum shown in (b). **(b)** Stimulated emission pumping spectrum of HCO prepared as described in (a).

Using the SEP technique, the linewidths (and therefore lifetimes) of the resonances can be measured. Many of the states live long enough so that not only the vibrational character of the level, but the rotational quantum numbers can be assigned.

Table 1 Experimental and Theoretical Linewidths for HCO Metastable States.

State	Energy (cm^{-1})	Linewidth (cm^{-1})			
		Experiment[a]	Experiment[c]	Theory[d]	Theory[e]
(0,4,0)	7428[a]	0.7		0.1	0.1
(0,3,2)	7643.7[a]	0.95		3.7	2.75
(0,4,1)	8390.5[a]	2.1		2.9	3.1
(0,3,3)	8547.9[a]	1.2		8.8	8.2
(0,5,0)	9091.97[a]	0.8		0.1	0.15
(0,5,1)	10153.1[a]	2.3		3.9	3.6
(0,4,3)	10432[a]	2.0		16	16.4
(0,6,0)	10836.1[a]	1.8	0.6	0.6	0.59
(0,5,2)	11194.7[a]	50	>15	25	31.4
(0,6,1)	11900[c]		5.5	6.9	5.6
(0,7,0)	12512[b]		0.9	1.5	1.86
(0,6,2)	12898[b]		13.5	16	
(0,7,1)	13590[c]		9.0	5.1	
(0,8,0)	14184[b]		1.3	3.7	
(0,9,0)	15900[c]		0.5		

a Adamson, Zhao, and Field (ref 19).
b Sappey and Crosley (ref 18).
c Neyer, Luo, Burak, and Houston (ref 70).
d Dixon (ref 46).
e Wang and Bowman (ref 49).

As predicted in calculations, the linewidths of the metastable states appear highly non-statistical and depend strongly on the vibrational character of the level excited. Table 1 presents both measured and calculated linewidths for a group of metastable resonances on the ground electronic state of HCO. The experimental measurements are upper bounds to the linewidth since the individual spin states of the radical could not be resolved. In general, resonances with only HC-O stretching character, $(0,v_2,0)$, have the narrowest linewidths, even at the highest energies measured.[69] Addition of HCO bending quanta (v_3) to HC-O stretching states increases the linewidth dramatically, implying a shorter lifetime. Theoretical calculations indicate that addition of H-CO stretch causes an even larger increase in the linewidth, but these have not been measured experimentally. It should also be noted that although these general trends are observed, the actual linewidths and the changes in the linewidths with vibrational character do not follow a consistent, quantitative pattern.

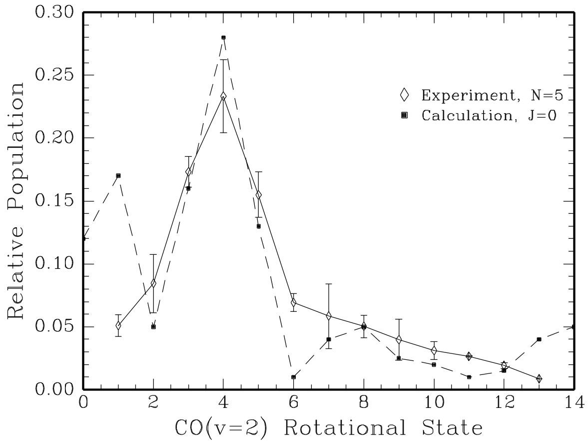

Figure 14 The CO(v=2) rotational population distribution obtained from the dissociation of the $\tilde{X}(0,7,0)$ state prepared by dumping on the $^{Q}R_0(5)$ transition shown in Figure 13(b). The solid line connects the experimental points (diamonds), and the error bars represent 2σ. The dashed line connects the points (squares) of the distribution calculated by Dixon for zero total angular momentum.

Product distributions have also been measured in a very detailed state-to-state experiment. The results of these experiments indicate that the SEP-prepared parent states (which have predominately C-O stretching character) produce vibrationally excited CO products. Only low rotational states are populated, and the distributions are structured (not thermal). The CO(v=2) rotational distribution from the dissociation of the N=5 level (the $J = N \pm ½$ spin states are not resolved in our SEP spectra) of the $\tilde{X}(0,7,0)$ resonance of HCO is shown in Figure 14. No CO in *v*=3 was detected from the dissociation of the (0,7,0) level. Interference from background CO in *v*=0 and 1 and/or lack of fragment population in these states has precluded measurement of these rotational distributions. These experimental results can be compared with the theoretical predictions of wavepacket calculations on the BBH surface performed by R. N. Dixon.[46] In contrast to experiment, Dixon's calculations predict that 64.5% of the CO products will be formed in *v*=3, with only 27.1% in *v*=2. However, Dixon's work does predict low rotational states of the CO to be populated in a non-thermal, structured distribution that agrees qualitatively quite well with experiment, as shown in Figure 14. Although there appears to be good agreement with experiment, it should be noted that the measured data is for *N*=5 while the calculation is for a total angular momentum of zero. It has been discovered that the rotational distributions of the fragment CO molecules depend not only on the vibrational character of the resonance but on the rotational state of the parent.

Rovibrational distributions of the CO products have been measured for the dissociation of other HCO vibrational resonances as well.[70] Figure 15 shows some of these measurements. In general, the rotational population is concentrated in the low *J* levels of the product, with some variation due to the vibrational state of the parent. There is however a change in the CO(*v*=3) population as different parent states are prepared. States with energies of 12,512 cm^{-1} (the (0,7,0) level) and

Figure 15 Product rotational distributions obtained for CO(*v*=2) and CO(*v*=3) following dissociation of HCO from *N* = 5 of the indicated resonance states. The error bars represent an uncertainty of 2σ.

below do not produce detectable amounts of CO(v=3), while parent states with energies of 12,898 cm^{-1} (the (0,6,2) level) and greater produce CO fragments in both v=2 and 3. This trend is also observed in Dixon's wavepacket calculations, but the energy at which the v=3 channel opens is lower. Significant population (>10%) in CO(v=3) is calculated for parent states with calculated energies of 12,106 cm^{-1} (his (0,6,1) level) and above. This discrepancy may be do to errors in the barrier height of the HCO surface. Further theoretical studies of this part of the surface and of the dissociation dynamics of these resonances are being conducted.[71]

Experiments using SEP preparation are providing dynamical probes of new sections of the ground state potential energy surface with very specific control of the vibrational energy and angular momentum. In contrast to the regions of the p.e.s. sampled by the Ã-state photodissociations, these experiments start with the H atom in the well of the HCO surface and with significant amount of stretching in the C-O coordinate. Comparison with dynamical calculations conducted on the BBH surface should allow even further insight into the accuracy of the potential. As discussed above, both time-dependent[45-47] and time-independent[34-37,43-44,49] quantum mechanical calculations have revealed fluctuations in the linewidths of these resonances, consistent with experiment. In addition, CO product distributions which are rotationally structured and vibrationally inverted have been predicted by theory. There has been no large calculational effort aimed at discerning parent rotational effects on the dissociation, although initial investigations of states with J=1 have shown interesting effects.[37] Continued theoretical interest[71] is also producing refinements to the potential energy surface which can be tested by these experimental results.

V. Conclusions

An accurate potential energy surface provides a very complete description of the forces at work in a chemical system. Creation of such a surface often depends on a strong interplay between theoretical and experimental methods of chemical physics. The HCO system provides an excellent example of how theory and experiment have pushed each other forward in an attempt to create such a description. Because of its importance in combustion, atmospheric, and interstellar chemistry, as well as the tractability of detailed measurements and accurate calculations on triatomic systems, HCO has been the focus of continued study.

Both theory and experiment have played vital roles in understanding the HCO system. The creation of a global p.e.s. for the $\tilde{X}$ state of HCO by Bowman, Bittman, and Harding required a large set of *ab initio* structure calculations along with empirical scaling based on the results of spectroscopic and kinetic experiments. Since its creation, the BBH surface has faced numerous tests of its accuracy and has held up reasonably well. Calculations employing the BBH surface have modeled the results of H+CO scattering experiments with fairly impressive accuracy and have reproduced many of the qualitative trends measured in HCO($\tilde{A}\leftarrow\tilde{X}$) photodissociation experiments. There are some discrepancies between the calculations and the experimental measurements, but the BBH surface has provided a base on which to analyze these differences. Theoretical calculations on the BBH p.e.s. were used to predict and characterize metastable resonances in the H+CO system which have now been identified experimentally. Highly non-statistical lifetimes and product state distributions from the decay of these resonances were also predicted from these calculations and have prompted continuing experiments which appear to support many of these predictions. The experiments, in turn, reveal further detailed dynamical information about the dissociation of these resonances which should prompt more theoretical modeling.

Due to the small size of the HCO system, very detailed dynamical information has been accessible both experimentally and theoretically, and although it is only triatomic, a large array of physical phenomena have been encountered and better understood through its study. The detailed shape of the potential energy surface, including the predicted presence of a metastable COH isomer, and its effects on inelastic cross sections of H+CO collisions have been investigated. Nonadiabatic electronic coupling due to Renner-Teller interactions and its effects on the lifetimes and dynamics of Ã-state predissociation have been studied in detail. Also the presence and non-statistical decay dynamics of metastable resonances on the ground electronic state of HCO have been predicted theoretically and measured experimentally. The story will certainly not end with the work presented here. For example, a new potential energy surface for the HCO system has recently been calculated, and dynamical predictions are currently underway.[71] Further experiments on H + CO collisions have also been recently performed.[55] The HCO system is thus continuing to provide an arena for the advancement of our theoretical and experimental understanding of chemical dynamics.

Acknowledgements

It is a pleasure to acknowledge the collaboration of many co-workers who contributed to the original papers describing the work summarized in this review. They include G. C. McBane, G. K. Chawla, G. C. Schatz, J-C. Loison, I. Burak, X. Luo, R. N. Dixon, E. Goldfield, and S. H. Kable. Itamar Burak and Scott Kable, in particular, were important not only in performing many of the experiments described but in helping to formulate an overall program which turned out to be more than the sum of its parts. We would like also to thank G. Ezra for helpful discussions of the HCO problem, and J. Bowman, R. Schinke and G. Flynn for preprints of their work. DWN would like to thank the Department of Education and IBM for graduate fellowship support. This work was supported by the National Science Foundation under Grant CHE-9224432 and by the Air Force Office of Scientific Research under Grant F49620-92-J-0080.

References

1. W. C. Gardiner, Jr., *Combustion Chemistry* (Springer-Verlag, New York, 1984), and references therein.

2. D. J. Hucknall, *Chemistry of Hydrocarbon Combustion* (Chapman and Hall, London, 1985), and references therein.

3. B. J. Finlayson-Pitts and J. N. Pitts, Jr., *Atmospheric Chemistry: Fundamentals and Experimental Techniques* (Wiley and Sons, New York, 1986), and references therein.

4. S. Chu and A. Balgarno, Proc. Roy. Soc. **342**, 194 (1975).

5. D. A. Ramsay, J. Chem. Phys. **21**, 960 (1953).

6. G. Herzberg and D. A. Ramsay, Proc. Roy. Soc. **A233**, 34 (1955).

7. J. W. C. Johns, S. H. Priddle, and D. A. Ramsay, Disc. Farad. Soc **35**, 90 (1963).

8. J. M. Brown and D. A. Ramsay, Can. J. Phys. **53**, 2232 (1975).

9. D. E. Milligan and M. E. Jacox, J. Chem. Phys. **51**, 277 (1969).

10. D. B. Oh, A. C. Stanton, and J. A. Silver, J. Phys. Chem. **97**, 2246 (1993).

11. R. König and J. Lademann, Chem. Phys. Lett. **94**, 152 (1983).

12. B. M. Stone, M. Noble, and E. K. C. Lee, Chem. Phys. Lett. **118**, 83 (1985).

13. G. Rumbles, J. J. Valentini, B. M. Stone, and E. K. C. Lee, J. Phys. Chem. **93**, 1303 (1989).

14. R. Vasudev and R. N. Zare, J. Chem. Phys. **76**, 5267 (1982).

15. G. Hall, A. G. Suits, and B. J. Whitaker, Chem. Phys. Lett. **203**, 277 (1993).

16. V. M. Vaidya, Proc. Roy. Soc. **147A**, 513 (1934).

17. V. M. Vaidya, Proc. Roy. Soc. **279A**, 572 (1964).

18. A. D. Sappey and D. R. Crosley, J. Chem. Phys. **93**, 7601 (1990).

19. G. W. Adamson, X. Zhao, and R. W. Field, J. Mol. Spec. **160**, 11 (1993); Proceedings of the 15th Combustion Research Conference (Chemistry Department, Brookhaven National Laboratory, Department of Energy).

20. J. B. Jeffries, D. R. Crosley, I. J. Wysong, and G. P. Smith, Proc. Symp. Int. Combust. **23**, 1847 (1991).

21. T. A. Cool and X-M. Song, J. Chem. Phys. **96**, 8675 (1992).

22. G. Caraccilol, T. H. Ellis, G. O. Este, A. Ruggolo, G. Scoles, and U. Valbusa, Astrophys. J. **229**, 451 (1979).

23. C. F. Wood, G. W. Flynn, and R. E. Weston, Jr., J. Chem. Phys. **77**, 4776 (1982).

24. C. A. Wight and S. R. Leone, J. Chem. Phys. **78**, 4875 (1983).

25. C. A. Wight and S. R. Leone, J. Chem. Phys. **79**, 4823 (1983).

26. J. M. Bowman, J. S. Bittman, and L. B. Harding, J. Chem. Phys. **85**, 911 (1986).

27. T. H. Dunning, J. Chem. Phys. **73**, 2304 (1980).

28. K. K. Murray, T. M. Miller, D. G. Leopold, and W. C. Lineberger, J. Chem. Phys. **84**, 2520 (1986).

29. H. Romanowski, K. T. Lee, J. M. Bowman, and L. B. Harding, J. Chem. Phys. **84**, 2520 (1986).

30. J. N. Murrell and J. A. Rodriguez, J. Mol. Struct. (Theochem) **139**, 267 (1986).

31. S. W. Cho, W. L. Hase, and K. N. Swamy, private commun.

32. L. C. Geiger and G. C. Schatz, J. Phys. Chem. **88**, 214 (1984).

33. L. C. Geiger, G. C. Schatz , and L. B. Harding, Chem. Phys. Lett. **114**, 520 (1985).

34. K.-T. Lee and J. M. Bowman, J. Chem. Phys. **85**, 6225 (1986); **86**, 215 (1987).

35. B. Gazdy, J. M. Bowman, and Q. Sun, Chem. Phys. Lett. **148**, 512 (1988).

36. B. Gazdy, and J. M. Bowman, Phys. Rev. A. **36**, 3083 (1987).

37. J. M. Bowman and B. Gazdy, Chem. Phys. Lett. **200**, 311 (1992).

38. L. C. Geiger, G. C. Schatz, and B. C. Garrett, in *Resonances in Electron-Molecule Scattering, van der Waals Complexes, and Reactive Chemical Dynamics*, edited by D. G. Truhlar (American Chemical Society, Washington, D.C., 1984), Chap. 22.

39. Y. H. Kim and D. A. Micha, J. Chem. Phys. **90**, 5486 (1989).

40. A. F. Wagner and J. M. Bowman, J. Phys. Chem. **91**, 5314 (1987).

41. R. S. Timonen, E. Ratajczak, D. Gutman, and A. F. Wagner, J. Phys. Chem. **91**, 5325 (1987).

42. L. B. Harding and A. F. Wagner, Proc. Int. Symp. Combust. **21**, 721 (1988).

43. B. Gazdy, J. M. Bowman, S-W. Cho, and A. F. Wagner, J. Chem. Phys. **94**, 4192 (1991).

44. S-W. Cho, A. F. Wagner, B. Gazdy, and J. M. Bowman, J. Chem. Phys. **96**, 2799 (1992); J. Chem. Phys. **96**, 2812 (1992); J. Chem. Phys. **95**, 9897 (1991).

45. S. K. Gray, J. Chem. Phys. **96**, 6543 (1992).

46. R. N. Dixon, J. Chem. Soc. Faraday Trans. **88**, 2575 (1992); Chem. Phys. Lett. **190**, 430 (1992).

47. E. M. Goldfield, S. K. Gray, and L. B. Harding, J. Chem. Phys. **99**, 5812 (1993).

48. M. R. Manaa and D. R. Yarkony, J. Chem. Phys. **100**, 473 (1994).

49. D. Wang and J. M. Bowman, J. Chem. Phys. **100**, 1021 (1994); B. Gazdy and J. M. Bowman, Adv. Mol. Vib. Collision Dyn. **1B**, 105 (1991).

50. See, for example, the article by S. K. Gray and E. Goldfield in this volume.

51. G. W. Flynn and R. E. Weston, Annu. Rev. Phys. Chem. **37**, 551 (1986).

52. S. A. Buntin, C. F. Geise, and W. R. Gentry, J. Chem. Phys. **87**, 1443 (1987).

53. A. Chattopadhyay, S. Tasaki, R. Bersohn, and M. Kawasaki, J. Chem. Phys., **95**, 1033 (1991).

54. M. A. Buntine, D. P. Baldwin, R. N. Zare, and D. W. Chandler, J. Chem. Phys., **94**, 4672 (1991).

55. C. K. Ni, G. W. Flynn, and S. Green, submitted.

56. G. K. Chawla, G. C. McBane, P. L. Houston, and G. C. Schatz, J. Chem. Phys. **88**, 5481-8 (1988).

57. G. C. McBane, S. H. Kable, P. L. Houston, and G. C. Schatz, J. Chem. Phys. **94**, 1141-1149 (1991).

58. R. Renner, Z. Phys. **92**, 172 (1934).

59. G. Duxbury, Chem. Soc. Spec. Per. Rep. Molec. Spectrosc. **3**, 497 (1975), and references therein.

60. Ch. Jungen and A. J. Merer, Mol. Phys. **40**, 1 (1980), and references therein.

61. R. N. Dixon, Mol. Phys. **54**, 333 (1985).

62. S. H. Kable, J.-C. Loison, P. L. Houston, and I. Burak, J. Chem. Phys. **92**, 6332-6333 (1990).

63. J.-C. Loison, S. H. Kable, P. L. Houston, and I. Burak, J. Chem. Phys. **94**, 1796-1802 (1991).

64. S. H. Kable, J.-C. Loison, D. W. Neyer, P. L. Houston, I. Burak, and R. N. Dixon, J. Phys. Chem. **95**, 8013 (1991).

65. D. W. Neyer, S. H. Kable, J.-C. Loison, P. L. Houston, I Burak, and E. M. Goldfield, J. Chem. Phys. **97**, 9036 (1992).

66. M. C. Chuang, M. F. Foltz, and C. B. Moore, J. Chem. Phys. **87**, 3855 (1987).

67. D. W. Neyer, X. Luo, P. L. Houston, and I. Burak, J. Chem. Phys. **97**, 9036-9045 (1992).

68. The lower figure is slightly different from that published in ref. 67. In the previously published figure the linewidths were affected by power broadening and the abscissa was slightly displaced from the true wavelengths.

69. The vibrational modes of the ground electronic state of HCO, which has a bent equilibrium geometry, are given in order of decreasing energy. The states are denoted by (v_1,v_2,v_3), where v_1, v_2, and v_3 are defined as the H-CO stretch, the HC-O stretch, and the bend, respectively.

70. D. W. Neyer, X. Luo, P. L. Houston, and I. Burak, in preparation.

71. H. J. Werner, P. Rosmus, and R. Schinke, private commun.